PCCP

Accepted Manuscript

ROYAL SOCIETY OF CHEMISTRY

www.rsc.org/pccp

Journal Name

RSCPublishing

ARTICLE

Thermal Lensing Effect of CS_2 Studied with Femtosecond Laser Pulses

Cite this: DOI: 10.1039/xoxxoooooox

Yi-Ci Li,[a] Yu-Ting Kuo,[a] Po-Yuan Huang,[a] Sidney S. Yang,[b] Cheng-I Lee,[c,†] and Tai-Huei Wei[a,†]

Received ooth January 2015,
Accepted ooth January 2015

DOI: 10.1039/xoxxoooooox

www.rsc.org/

By chopping 820 nm 18 femtosecond (fs)-laser pulses, continuously generated by a self-mode locked Ti:Al_2O_3 laser at 82 MHz, into trains with both train-width and train-to-train separation considerably longer than CS_2's thermal diffusivity time constant τ_{th}, we conducted *Z*-scan measurements on it at various times relative to the leading pulse of each train (*T*'s). As a result, we observed negative nonlinear refraction strengthening with *T* within τ_{th} and gradually turning steady with *T* exceeding τ_{th}. We quantitatively explain the experimental results in terms of the thermal lensing effect. In particular, we attribute the heat generation to non-radiative relaxation of libration excited by individual 18 fs-pulses via stimulated Raman scattering. Different from the common view of multi-photon excitation, we propose and verify a new heat-generating mechanism for thermal lensing effect in CS_2.

1. Introduction

The thermal lensing effect induced in various simple liquids by femtosecond (fs) laser pulses delivered at repetition rates of tens of MHz has been studied with the *Z*-scan technique [1−7]. When the nanosecond (ns) order pulse-to-pulse separations $\tau_{p\text{-}p}$'s (reciprocal of the repetition rates) are considerably shorter than the sub-millisecond (sub-ms) to ms order thermal diffusivity time constant τ_{th} [8], the observed negative lensing effect, which strengthens with time relative to the leading pulse (denoted by *T*) within τ_{th} and gradually turns steady with *T* exceeding τ_{th}, is ascribed to the thermal lensing effect. The multi-photon excitation processes have been commonly offered to explain the heat generation [1−7,9].

In this study we further explore the mechanism of thermal lensing effect induced in CS_2, an example of simple liquids. In the experimental aspect, we used a self-mode locked Ti:Al_2O_3 laser which continuously delivers TEM_{00} mode laser pulses at a repetition rate of 82 MHz. These pulses have a central wavelength of λ_c=820 nm (equivalently a central angular frequency of ω_c=2.3×10^{15} s^{-1}) and a duration of τ=18 fs, measured at half-width at e^{-1} maximum (HWe^{-1}M). By chopping the continuously generated pulses into trains with a train-width of τ_t=41 ms and a train-to-train separation of $\tau_{t\text{-}t}$=0.18 s (Fig. 1), both being longer than CS_2's τ_{th}, we found with the *Z*-scan technique that the thermal lensing effect in it evolves with *T* in the same manner as the above-mentioned simple liquids. In the theoretical aspect, we quantitatively explain the thermal lensing effect induced in CS_2 in terms of excitation of molecular motions by individual 18 fs-laser pulses, heat generation due to relaxation of the excited molecular motions, sample density change due to heat accumulated across neighboring pulses and thermal diffusivity. In particular, while CS_2 is free from linear absorption (LA) and two-photon absorption (TPA) of the 18 fs-pulses at 820 nm (Fig. 2), we attribute the heat generation to non-radiative relaxation of libration excited by individual 18 fs-laser pulses via

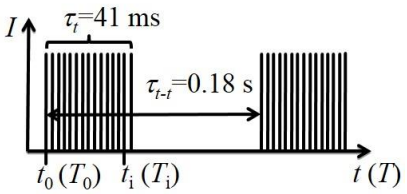

Fig. 1. The temporal profile of the 18 fs-pulse trains. *t* denotes the time in the laboratory reference frame and t_i specifies the arrival time of the ith pulse ($0 \le i \le i_{end}$ with i_{end}=41 ms/$\tau_{p\text{-}p}$) at a reference position *z*. $T \equiv t - t_0$ and $T_i \equiv t_i - t_0$ correspond to *t* and t_i measured relative to t_0.

stimulated Raman scattering (SRS), a kind of stimulated light scattering (SLS) process. Here libration means the vibrational motion of entire individual molecules with respect to surrounding molecules, different from the atomic vibration within individual molecules, referred to as intra-molecular vibration or simply vibration.

According to previous studies of time-resolved optical Kerr effect (OKE) [10−23] in a variety of simple liquids, resonant excitations of both intra- and inter-molecular motions, in addition to non-resonant excitation of electronic motion, can be fulfilled by fs laser pulses via various SLS processes (third-order nonlinear optical responses to the fs laser pulses). Excitation of each molecular motion by means of a specific SLS process promotes individual molecules from state $|0)_m$ to state $|1)_m$, via an intermediate virtue state, by absorbing a photon at angular frequency ω_1 and emitting a photon at angular frequency ω_2 with ($\omega_1 - \omega_2$) falling within the range [$\Omega_m - \Delta\Omega_m/2$, $\Omega_m + \Delta\Omega_m/2$]. Here Ω_m and $\Delta\Omega_m$ respectively denote the band center energy, relative

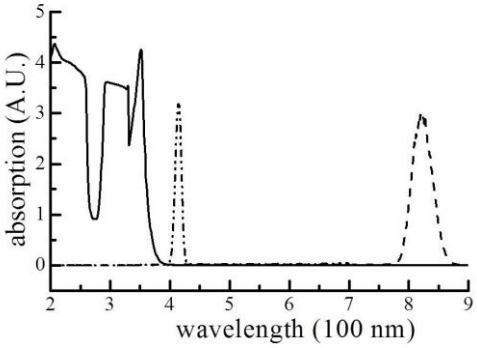

Fig. 2. Linear absorption spectrum of CS_2 measured by a spectrophotometer (solid line). The dashed and dash-dotted lines represent the spectrum of the 820 nm 18 fs-pulses and that of the pulses after frequency doubling. Transparency at both ~410 and ~820 nm rules out LA and TPA of 820 nm incident pulses.

to state $|0)_m$, and band width of state $|1)_m$ with the Planck′s constant $\hbar$ divided out (Fig. 3). The subscript m (=v, l, d and p respectively) specifies the molecular motions: v for vibration, l for libration, d for diffusive reorientation and p for polarizability distortion. The SLS processes responsible for excitations of vibration and libration are called SRS and those for excitations of diffusive reorientation and polarizability distortion are called stimulated Rayleigh-wing scattering [24]. Note that each kind of molecular motions may include various modes; however, we only consider one mode associated with it in this study. For example, CS_2′s vibration contains a symmetric stretching, an asymmetric stretching and two bending modes; however, we only consider the symmetric stretching mode (*vide infra*). Since both ω_1 and ω_2 are required to fall within the spectrum of a pulse to induce a SLS process, excitation of the corresponding molecular motion demands that the pulse have a spectrum width ($\Delta\omega$), measured at half-width at e^{-1} maximum (HWe^{-1}M), comparable or larger than the band center energy Ω_m of the excited state. Fs pulses were used in these studies because their wide spectra help to unravel sufficient excited molecular motions.

Here we are particularly interested in excess energy of these excited molecular motions which is converted from the absorbed pulse energy and eventually turned into heat to activate the thermal lensing effect. Typical Ω_m′s for excited inter-molecular motions of simple liquids are in the order of 10^{12} s^{-1} (tens of cm^{-1} in wavenumber) for excited libration and 10^{10}–10^{11} s^{-1} (sub cm^{-1} to cm^{-1} in wavenumber) for both excited diffusive reorientation and excited polarizability distortion. They are greatly smaller than that for excited vibration (Ω_v), in the order of 10^{14} s^{-1} (hundreds to a thousand and some cm^{-1} in wavenumber) [25]. Provided that all molecular motions can be excited with comparable probability, non-radiative relaxation of excited vibration with the largest Ω_m predominantly contribute to the thermal lensing effect. This is because a vibrationally excited molecule can release considerably more excess energy (Ω_v) than a molecule excited by other means. However, when the spectrum width ($\Delta\omega$) of an 18 fs-laser pulse is considerably larger than the typical Ω_m′s of the excited inter-molecular motions, it tends to be smaller than the typical Ω_v. This makes vibration less likely to be excited by an 18 fs-laser pulse. Under this circumstance, relaxation of excited inter-molecular motions may play a role, even a dominant role, in heat generation.

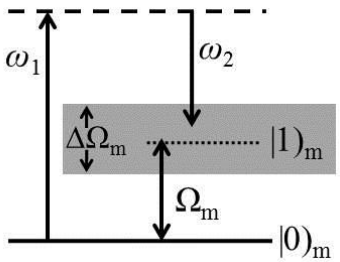

Fig. 3. The diagram of a SLS-induced molecular excitation from state $|0)_m$ to state $|1)_m$. Ω_m and $\Delta\Omega_m$ denote the band center energy, relative to $|0)_m$, and band width of state $|1)_m$ with the Planck′s constant $\hbar$ divided out.

Absorption of a TEM_{00} mode 18 fs-pulse, by the sample (CS_2) via the SLS processes, causes a temperature gradient ($\nabla\theta$) which drives in the sample an acoustic wave, namely thermal acoustic wave, propagating in the lateral direction at a speed of v_s in the order of 1000 m/s [26]. This wave renders a sample density change $\Delta\rho$ which predominantly contributes to the thermal lensing effect [27]. Since $\Delta\rho$ becomes noticeable after the acoustic wave propagates across the beam cross-section in the transit-time τ_{ac} ($\equiv w_0/v_s$ with w_0 denoting the beam radius at the waist) estimated in 10 ns order (*vide infra*) [28], an 18 fs-pulse with its duration greatly shorter than τ_{ac} does not experience the thermal lensing effect induced by itself. However, it experiences the thermal lensing effect induced by pulses prior to it because the pulse-to-pulse separation of τ_{p-p}=12.2 ns ((82 MHz)$^{-1}$) is comparable with τ_{ac} but greatly shorter than τ_{th} in the sub-ps to ms order [8].

Because the train width τ_t=41 ms is considerably longer than τ_{th} of the sample (CS_2), the thermal lensing effect built up across neighboring pulses is gradually suppressed and balanced by thermal diffusivity. On the other hand, because τ_{t-t} is significantly longer than τ_{th}, the sample (CS_2) thermally perturbed by a certain pulse train returns to thermodynamic (thermal, mechanical and chemical) equilibrium before the next pulse train arrives.

2. Experimental

The *Z*-scan technique (Fig. 4) has already been described elsewhere in detail [8]. Briefly, a shutter is placed in the light path before the beam splitter BS1 to chop the 82 MHz 18 fs-pulses into trains with τ_t=41 ms and τ_{t-t}=0.18 s. A fraction of the pulse trains, propagating along the +*z* axis, is then split by BS1 and directed to detector D1, which monitors the input power fluctuation. The major portion of the pulse trains passing BS1 is tightly focused to the waist at *z*=0 of radius $w_0 \equiv w(0)$=14.0 μm half-width at e^{-2} maximum (HWe^{-2}M). Each pulse train transmitted through the sample at a certain position *z* relative to the beam waist is split into two by the beam splitter BS2 and directed to detector D2 and the apertured detector D3, which respectively monitor the total and axial transmitted powers. Detectors D1, D2 and D3 take measurements at 10 different times relative to the leading pulse of the train: *T*=1, 2, 3, 5, 7, 9, 11, 21, 31, and 41 ms respectively. Outputs of D2 and D3 are divided by that of D1 and recorded as functions of *z*. The ratios D2/D1 and D3/D1, after being normalized with those in the linear regime (regions of large |*z*|), are respectively referred to as

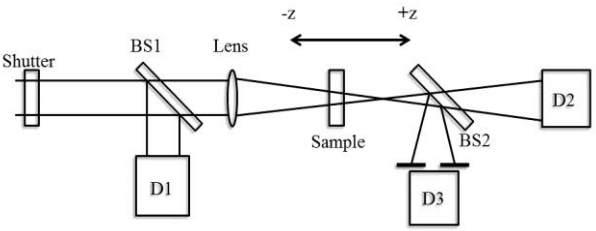

Fig. 4. The *Z*-scan setup which records the total and axial transmittances as functions of the sample position *z*.

the normalized transmittance (*NT*) and normalized axial transmittance (NT_a). When *NT* reflects nonlinear absorption (NLA) alone, NT_a involves nonlinear refraction (NLR) in combination with NLA (if present). Plots of *NT* and NT_a as functions of *z* are named the "open aperture" and "closed aperture" *Z*-scan curves respectively. When NLA is noticeable in NT_a, we can effectively eliminate it by dividing NT_a by *NT*. The plot of NT_a/NT as a function of *z*, namely the divided *Z*-scan curve, shows the sign of the lensing effect. When NLA is absent or negligibly small in NT_a, the closed aperture *Z*-scan curves themselves show the signs of the lensing effect. The lensing effect, either positive or negative, arises from the dependence of a sample's refractive index change Δn on time-domain intensity *I* (energy per unit area per unit time), frequency-domain intensity *I′*(energy per unit area per unit angular frequency) or generalized fluence ($F_G \equiv \int I dt$). The negative lensing effect (i.e., Δn has a minimum at the beam center (r=0) for a TEM_{00} mode pulse) of a sample renders a peak on the $-z$ side and a valley on the $+z$ side in a divided or closed aperture *Z*-scan curve. This is because it slows the light speed least at the beam center. Thus, it lessens the beam divergence at the aperture in front of D3 when the sample is before the beam waist and augments the beam divergence when the sample is after the beam waist.

In this study, the sample was contained in a quartz cuvette with a thickness of L=0.1 cm. The aperture (0.3 cm in radius) was placed at 22.5 cm after the beam waist. This allows 67% of the power at the aperture plane to reach D3 when the sample is placed in the linear regime (far from the location of the beam waist). The aperture radius remained unchanged in the course of *Z*-scan measurements.

Consider a pulse train propagates along the $+z$ direction without the sample in the light path. In the laboratory reference frame, the time-domain electric field strength of the ith pulse $\vec{E}_0^{(i)}(z,r,t)$ ($0 \le i \le i_{end}$ with i_{end}=41 ms/τ_{p-p}) in the train (Fig. 1) can be expressed as the Fourier transform of the corresponding frequency-domain electric field strength $\vec{E}_0^{\prime(i)}(z,r,\omega)$ [29]

$$\vec{E}_0^{(i)}(z,r,t) = \frac{1}{2\pi}\int_{-\infty}^{\infty} \vec{E}_0^{\prime(i)}(z,r,\omega)\times e^{i\omega t} d\omega \,. \quad (1)$$

Here t denotes the time, r refers to the lateral distribution of the ith pulse and $\omega = 2\pi c/\lambda$ is the angular frequency with c and λ being the light speed and wavelength pertaining to free space. Since each pulse in a train is identical, $\vec{E}_0^{(0)}(z,r,t)$ equals $\vec{E}_0^{(i)}(z,r,t+T_i)$ with $T_i \equiv t_i - t_0 = i\times\tau_{p\text{-}p}$ being the time difference between the peaks of the ith pulse and the leading pulse (i=0). Here we let t_i and t_0 denote the arrival times of the peaks of the ith and the leading pulses at z. Since $\vec{E}_0^{(i)}(z,r,t)$ is necessarily real, $\vec{E}_0^{\prime(i)}(z,r,\omega)$ is a Hermitian complex quantity, i.e., its real and imaginary parts are respectively symmetrical and anti-symmetrical about ω=0. Referring to Ref.[30] for z and r dependence of a monochromatic TEM_{00} mode laser beam, we write $\vec{E}_0^{\prime(i)}(z,r,\omega)$ in eq.(1) as

$$\vec{E}_0^{\prime(i)}(z,r,\omega) = \frac{w_0}{w(z,\omega)}\times \vec{E}_0^{\prime(i)}(0,0,\omega_c)\times e^{-\left(\frac{\omega\pm\omega_c}{\sqrt{2}\Delta\omega}\right)^2}\times e^{-\left[\frac{r}{w(z,\omega)}\right]^2} \times e^{-i\phi_0^{(i)}(z,r,\omega)}\times e^{-i(kz+\omega T_i)} \quad (2)$$

where $w(z,\omega)=w_0\times[1+(z/z_0)^2]^{1/2}$ is the beam radius (HW1/e^2M) at z with w_0 (14.0 μm) being $w(0)$ and $z_0(\omega)=\pi w_0^2/\lambda$ is the diffraction length of the ω component of the laser beam in free space. $\vec{E}_0^{\prime(i)}(0,0,\omega_c)$, with ω_c being the central angular frequency 2.3×10^{15} s^{-1}, is the frequency-domain on-axis electric field strength, a real quantity equal to $\vec{E}_0^{\prime(i)}(0,0,-\omega_c)$, of the ith pulse at z=0 and $\omega=\omega_c$, and

$$\phi_0^{(i)}(z,r,\omega) = \frac{kr^2}{2R(z,\omega)} - \tan^{-1}\left[\frac{z}{z_0(\omega)}\right] \quad (3)$$

is the phase slowly varying with z, in contrast to kz rapidly varying with z. $R(z,\omega)=z\times\{1+[z_0(\omega)/z]^2\}$ is the curvature radius of the wave front at z. $k=\omega/c$ denotes the wave propagation number. The term $\exp\{-[(\omega\pm\omega_c)/\sqrt{2}\Delta\omega]^2\}$ is used to ensure the Gaussian distribution of $\vec{E}_0^{(i)}(z,r,t)$ in t (*vide infra*). Here the "+" and "–" signs before ω_c are employed when ω is negative and positive respectively. The term $\exp(-i\omega T_i)$ is introduced to ensure that $\vec{E}_0^{(i)}(z,r,t+T_i)$ equals $\vec{E}_0^{(0)}(z,r,t)$. In eqs.(1) and (2), ω can be either positive or negative. k, λ and z_0 are of the same sign as ω. λ_c and ω_c are both positive. Besides, $\phi_0^{(i)}$ and R are anti-symmetrical about ω=0. By integrating eq.(1), with eqs.(2) and (3) substituted in, we obtain

$$\vec{E}_0^{(i)}(z,r,t) = \mathrm{Re}\left\{\sqrt{\frac{2}{\pi}}\times\frac{\Delta\omega\cdot w_0}{w(z,\omega_c)}\times\vec{E}_0^{\prime(i)}(0,0,\omega_c)\times e^{-\left(\frac{t-T_i-z/c}{\sqrt{2}\tau}\right)^2} \times e^{-\left[\frac{r}{w(z,\omega_c)}\right]^2}\times e^{-i\phi_0^{(i)}(z,r,\omega_c)}\times e^{\{-i[k_c z-\omega_c(t-T_i)]\}}\right\} \quad (4)$$

with $\tau=1/\Delta\omega$. In this integration, we consider change of the term $\exp\{-[(\omega\pm\omega_c)/\sqrt{2}\Delta\omega]^2\}$ in eq.(2) with ω; however, we ignore the dependence of w and $\phi_0^{(i)}$ on ω and regard them as functions of ω_c. Accordingly, we add the subscript "c" to the argument ω of w and $\phi_0^{(i)}$ in eq.(4). Since, in the derivation of eq.(4) from eqs.(1)–(3), the slowly varying phase $\phi_0^{(i)}$ is regarded as ω independent and k in the rapidly varying phase term ($kz+\omega T_i$) is linearly proportional to ω, eqs.(2) and (4) represent a transform limited pulse [31]. Moreover, since our autocorrelation and spectrum measurements, conducted before BS1, respectively show τ=18 fs and $\Delta\omega=5.5\times10^{13}$ s^{-1} whose product equals one, we ignore chirping induced in the components before BS1 due to nonzero 2nd order derivative of k with respect to ω ($d^2k/d\omega^2$) and thus assume the pulse remains transform limited till the position immediately before BS1. In the following we further ignore chirping induced in BS1 and the lens to make eqs.(2) and (4) suitable for the sample traveling between the lens and BS2. According to eq.(4), $t_i=z/c+T_i$ denotes the arrival time of the ith pulse's peak at z.

By integrating the magnitude of Poynting vector ($|\vec{S}^{(i)}| = c\varepsilon_0 \left|\vec{E}_0^{(i)}(z,r,t)\right|^2$) of the ith pulse over its duration, we obtain, according to eq.(1), the fluence (energy per unit area)

$$F_0^{(i)}(z,r)=\frac{c\varepsilon_0}{4\pi^2}\int_{-\infty}^{\infty}\left|\int_{-\infty}^{\infty}\vec{E}_0'^{(i)}(z,r,\omega)\times e^{i\omega t}d\omega\right|^2 dt$$
$$=\frac{c\varepsilon_0}{2\pi}\int_{-\infty}^{\infty}\vec{E}_0'^{(i)}(z,r,\omega)\times\vec{E}_0'^{(i)*}(z,r,\omega)d\omega$$
$$=\frac{c\varepsilon_0}{2\pi}\int_{-\infty}^{\infty}\vec{E}_0''^{(i)}(z,r,\omega)\times\vec{E}_0''^{(i)*}(z,r,\omega)d\omega \quad (5)$$
$$=\int_{-\infty}^{\infty}I_0'^{(i)}(z,r,\omega)d\omega$$

Here ε_0 denotes the electric permittivity of free space and equals 8.85×10^{-12} $C^2/(N\times m^2)$, $\vec{E}_0''^{(i)}(z,r,\omega)=\vec{E}_0'^{(i)}(z,r,\omega)\times e^{i(kz+\omega T_i)}$ represents the slowly varying amplitude of $\vec{E}_0'^{(i)}(z,r,\omega)$, and

$$I_0'^{(i)}(z,r,\omega)=\frac{c\varepsilon_0}{2\pi}\vec{E}_0''^{(i)}(z,r,\omega)\times\vec{E}_0''^{(i)*}(z,r,\omega)$$
$$=\left[\frac{w_0}{w(z,\omega)}\right]^2\times I_0'^{(i)}(0,0,\omega_c)\times e^{-\left(\frac{\omega\pm\omega_c}{\Delta\omega}\right)^2}\times e^{-\frac{2r^2}{w^2(z,\omega)}} \quad (6)$$

is the frequency-domain intensity. Here $I'_0{}^{(i)}(0,0,\omega_c)=c\varepsilon_0\left|\vec{E}_0''^{(i)}(0,0,\omega_c)\right|^2/2\pi$ denotes the frequency-domain on-axis intensity of the ith pulse at z=0 and $\omega=\omega_c$. Since $\vec{E}_0''^{(i)}(z,r,\omega)$ is Hermitian, similar to $\vec{E}_0'^{(i)}(z,r,\omega)$, $I'_0{}^{(i)}(z,r,\omega)$ equals $I'_0{}^{(i)}(z,r,-\omega)$ and thus eq.(5) can be rewritten as

$$F_0^{(i)}(z,r)=2\int_0^{\infty}I_0'^{(i)}(z,r,\omega)d\omega. \quad (7)$$

By integrating eq.(7), with eq.(6) substituted in, over the whole beam cross section we obtain the pulse energy of the ith pulse

$$\varepsilon_0^{(i)}=\int_0^{\infty}F_0^{(i)}(z,r)\times2\pi r dr$$
$$=2\int_0^{\infty}\int_0^{\infty}I_0'^{(i)}(z,r,\omega)d\omega\times2\pi r dr=\pi^{3/2}w_0^2\Delta\omega I_0'^{(i)}(0,0,\omega_c) \quad (8)$$

Accordingly, we can relate $I_0'^{(i)}(0,0,\omega_c)$ to $\varepsilon_0^{(i)}$ as

$$I_0'^{(i)}(0,0,\omega_c)=\frac{\varepsilon_0^{(i)}}{\pi^{3/2}w_0^2\Delta\omega}. \quad (9)$$

Given an average power P_{avg} for the 82 MHz 18 fs-laser pulses, $\varepsilon_0^{(i)}$ equals P_{avg}/82 MHz for all the i values.

3. Theoretical model

The frequency-domain electromagnetic wave equation driven by the third-order nonlinear polarization $\vec{P}'^{(3,i)}(z,r,\omega)$ is [32]

$$\nabla\left[\nabla\cdot\vec{E}'^{(i)}(z,r,\omega)\right]-\nabla^2\vec{E}'^{(i)}(z,r,\omega)-\frac{\omega^2}{c^2}\vec{E}'^{(i)}(z,r,\omega)$$
$$=\mu\omega^2\vec{P}'^{(3,i)}(z,r,\omega) \quad (10)$$

where μ represents the magnetic permeability of the sample (CS_2), nearly equal to that of the vacuum (μ_0) since the sample is nonmagnetic. The sample position z ranges between z_f and z_f+L with z_f denoting its front surface position relative to the beam waist.

Since $\vec{E}'^{(i)}$ is a quasi-plane wave disturbance with $\nabla\cdot\vec{E}'^{(i)}\sim0$, $\vec{E}_0''^{(i)}(z,r,\omega)$ varies with z much more slowly than e^{-ikz}, and the sample satisfies the thin sample condition with its thickness 0.1 cm less than the diffraction length of the ω_c component of the pulse in it ($n\times z_0(\omega_c)$=0.12 cm with n=1.63 being CS_2's refractive index [26] and $z_0(\omega_c)=7.5\times10^{-2}$ cm being the diffraction length in free space), we simplify eq.(10) as

$$2ik\frac{\partial\vec{E}''^{(i)}(z,r,\omega)}{\partial z}=\mu\omega^2\vec{P}''^{(3,i)}(z,r,\omega), \quad (11)$$

with $\vec{P}''^{(3,i)}(z,r,\omega)=\vec{P}'^{(3,i)}(z,r,\omega)\times e^{i(kz+\omega T_i)}$ denoting the slowly varying amplitude of $\vec{P}'^{(3,i)}(z,r,\omega)$. The detailed derivation of eq.(11) from eq.(10) is shown in Part A of the Supporting Information (SI).

In the following, we deal with one of the SLS-excited inter-molecular motions: libration. Likewise, we can deal with the other two inter-molecular motions (diffusive reorientation and polarizability distortion) and the intra-molecular vibration.

As explained in Part A of the SI, excitation of libration via SRS results in a third-order nonlinear polarization

$$\vec{P}''^{(3,i)}(z,r,\omega)=2\varepsilon_0\times\int_0^{\infty}\tilde{\chi}^{(3)}(\omega;\omega,\omega_a,-\omega_a)\vdots\vec{E}''^{(i)}(z,r,\omega)$$
$$\cdot\left|\vec{E}''^{(i)}(z,r,\omega_a)\right|^2 d\omega_a \quad (12)$$

Here $\tilde{\chi}^{(3)}(\omega;\omega,\omega_a,-\omega_a)$ is nonzero only when ω_a falls within the range [ω–Ω_l–$\Delta\Omega_l$/2, ω–Ω_l+$\Delta\Omega_l$/2] or [ω+Ω_l–$\Delta\Omega_l$/2, ω+Ω_l+$\Delta\Omega_l$/2]. In the following, we consider the situation that ω is positive and let ω_l and ω_h denote ω_a in the ranges [0, ω] and [ω, ∞] respectively. Accordingly, we can rewrite eq.(12) as

$$\vec{P}''^{(3,i)}(z,r,\omega)=2\varepsilon_0\times\begin{bmatrix}\int_0^{\omega}\tilde{\chi}^{(3)}(\omega;\omega,\omega_l,-\omega_l)\vdots\vec{E}''^{(i)}(z,r,\omega)\\ \cdot\left|\vec{E}''^{(i)}(z,r,\omega_l)\right|^2 d\omega_l\\ +\int_{\omega}^{\infty}\tilde{\chi}^{(3)}(\omega;\omega,\omega_h,-\omega_h)\vdots\vec{E}''^{(i)}(z,r,\omega)\\ \cdot\left|\vec{E}''^{(i)}(z,r,\omega_h)\right|^2 d\omega_h\end{bmatrix}. \quad (13)$$

In order for $\vec{P}''^{(3,i)}(z,r,\omega)$ to be nonzero, ω_l within the range [ω–Ω_l–$\Delta\Omega_l$/2, ω–Ω_l+$\Delta\Omega_l$/2] needs to be covered in the spectrum of $\vec{E}''^{(i)}(z,r,\omega)$ with ω, or ω_h within the range [ω+Ω_l–$\Delta\Omega_l$/2, ω+Ω_l+$\Delta\Omega_l$/2] needs to be covered in the spectrum of $\vec{E}''^{(i)}(z,r,\omega)$ with ω. Note that $\tilde{\chi}^{(3)}(\omega;\omega,\omega_l,-\omega_l)$ equals $\tilde{\chi}^{(3)*}(\omega;\omega,\omega_h,-\omega_h)$ if (ω–ω_l) equals –(ω–ω_h) (see the paragraph below eq.(S10) in the SI). Given $\Delta\omega$ (5.5×10^{13} s^{-1}) considerably smaller than Ω_v (1.2×10^{14} s^{-1}, *vide infra*), we can hardly find ω_l within the range [ω–Ω_v–$\Delta\Omega_v$/2, ω–Ω_v+$\Delta\Omega_v$/2] or ω_h within the range [ω+Ω_v–$\Delta\Omega_v$/2, ω+Ω_v+$\Delta\Omega_v$/2] falling in the spectrum of $\vec{E}''^{(i)}(z,r,\omega)$ with ω. This signifies that $\vec{P}''^{(3,i)}(z,r,\omega)$ pertaining to vibrational excitation via SRS tends to be zero. In other words, an 18 fs-laser pulse can barely excite the vibration.

By substituting eq.(13) into eq.(11), we can deduce the wave equation [24,29,32]

$$\frac{\partial\vec{E}''^{(i)}(z,r,\omega)}{\partial z}=-\frac{i2\pi k}{c\varepsilon_0}\times\begin{bmatrix}\int_0^{\omega}\tilde{\chi}^{(3)}(\omega;\omega,\omega_l,-\omega_l)\\ \cdot I'^{(i)}(z,r,\omega_l)\cdot\vec{E}''^{(i)}(z,r,\omega)d\omega_l\\ +\int_{\omega}^{\infty}\tilde{\chi}^{(3)}(\omega;\omega,\omega_h,-\omega_h)\\ \cdot I'^{(i)}(z,r,\omega_h)\cdot\vec{E}''^{(i)}(z,r,\omega)d\omega_h\end{bmatrix}. \quad (14)$$

Here we have replaced $\left|\vec{E}''^{(i)}(z,r,\omega_{l(h)})\right|^2$ by $2\pi I'^{(i)}(z,r,\omega_{l(h)})/c\varepsilon_0$ according to eq.(5). By further expressing $\vec{E}''^{(i)}(z,r,\omega)$ as $\vec{A}^{(i)}(z,r,\omega)\times e^{-i\phi^{(i)}(z,r,\omega)}$ and thus $I'^{(i)}(z,r,\omega)$ as $c\varepsilon_0\left|\vec{A}^{(i)}(z,r,\omega)\right|^2/2\pi$, we can separate eq.(14) into two terms, one for NLA and the other for NLR,

$$\frac{\partial I'^{(i)}_{z_f}(z',r,\omega)}{\partial z'} = -2k\begin{bmatrix}\int_0^{\omega}\beta_l I'^{(i)}_{z_f}(z',r,\omega_l)\times I'^{(i)}_{z_f}(z',r,\omega)d\omega_l \\ -\int_{\omega}^{\infty}\beta_h I'^{(i)}_{z_f}(z',r,\omega_h)\times I'^{(i)}_{z_f}(z',r,\omega)d\omega_h\end{bmatrix} \quad (15)$$

and

$$\frac{\partial \phi^{(i)}_{z_f}(z',r,\omega)}{\partial z'} = k\begin{bmatrix}\int_0^{\omega} n_{2l} I'^{(i)}_{z_f}(z',r,\omega_l)d\omega_l \\ +\int_{\omega}^{\infty} n_{2h} I'^{(i)}_{z_f}(z',r,\omega_h)d\omega_h\end{bmatrix} + k\Delta n^{(i)}_{z_f}(z',r) \quad (16)$$

excluding the last term on the right hand side of eq.(16). Note that in the derivation of eqs.(15) and (16) from eq.(14), we have used $z=z_f+z'$ with z' denoting the penetration depth of the ith pulse into the sample. z_f, as was mentioned in the paragraph after eq.(10), represents the sample front surface position relative to the beam waist. Here $\beta_l \equiv -2\pi\tilde{\chi}^{(3)}_{Im}(\omega;\omega,\omega_l,-\omega_l)/c\varepsilon_0$ and $\beta_h \equiv 2\pi\tilde{\chi}^{(3)}_{Im}(\omega;\omega,\omega_h,-\omega_h)/c\varepsilon_0$ are the third-order NLA coefficients; $n_{2l} \equiv 2\pi\tilde{\chi}^{(3)}_{Re}(\omega;\omega,\omega_l,-\omega_l)/c\varepsilon_0$ and $n_{2h} \equiv 2\pi\tilde{\chi}^{(3)}_{Re}(\omega;\omega,\omega_h,-\omega_h)/c\varepsilon_0$ are the third-order NLR coefficients. Since $\tilde{\chi}^{(3)}(\omega;\omega,\omega_l,-\omega_l)$ equals $\tilde{\chi}^{(3)*}(\omega;\omega,\omega_h,-\omega_h)$ if $(\omega-\omega_l)$ equals $-(\omega-\omega_h)$, $\beta_h=-\beta_l$ and $n_{2h}=n_{2l}$ in case $(\omega-\omega_l)$ equals $-(\omega-\omega_h)$.

Considering absorption of individual 18 fs-pulses by the sample induces the thermal lensing effect and, because the thermal diffusivity time constant of τ_{th}=408 μs (*vide infra*) for CS_2 is greatly longer than the pulse-to-pulse separation of τ_{p-p}= 12.2 ns, this effect is sustained to and experienced by the subsequent pulses, we introduce the term $k\Delta n^{(i)}_{z_f}$ on the right hand side of eq.(16) to represent the thermal lensing effect. Here $\Delta n^{(i)}_{z_f}$ denotes the thermally induced refractive index change by the 0th through the (i–1)th pulses and experienced by the ith pulse (i>0). Note that $\Delta n^{(0)}_{z_f}$ equals 0 because the sample is in full thermodynamic equilibrium when the leading pulse (i=0) starts to interact with the sample.

To derive $\Delta n^{(i)}_{z_f}$ for i≥1, we evaluate the heat generated in a unit of volume of the sample by the (i–1)th pulse (i>0), via the ps order non-radiative $|1\rangle_l \rightsquigarrow |0\rangle_l$ relaxation [11], by integrating eq.(15) over ω. This yields

$$\delta Q^{(i-1)}_{z_f}(z',r) = 2\int_0^{\infty}\frac{\partial I'^{(i-1)}_{z_f}(z',r,\omega)}{\partial z'}d\omega \quad (17)$$

which results in a temperature rise

$$\delta\theta^{(i-1)}_{z_f}(z',r) = \frac{\delta Q^{(i-1)}_{z_f}(z',r)}{\rho^{(i-1)}_{z_f}(z',r)\times c_p}. \quad (18)$$

Here $\rho^{(i-1)}_{z_f}(z',r)$ is the sample density experienced by the (i–1)th pulse and c_p denotes the sample isobaric specific heat. By including the effect of thermal diffusivity, we relate the sample temperature $\theta_{z_f}(z',r,t)$ to $\theta^{(i-1)}_{z_f}(z',r)$ (= $\theta_{z_f}(z',r,t_{i-1})$), the temperature experienced by the (i–1)th pulse as

$$\theta_{z_f}(z',r,t) = \theta^{(i-1)}_{z_f}(z',r) + \delta\theta^{(i-1)}_{z_f}(z',r) + \int_{t_{i-1}}^{t} D_{th}\nabla^2\theta_{z_f}(z',r,t')dt'. \quad (19)$$

This relation holds for t ranging between t_{i-1} and t_i which respectively denote the arrival times of the peaks of the (i–1)th and the ith pulses at the sample position $z=z_f+z'$. Provided that $\theta^{(i-1)}_{z_f}(z',r)$ and $\rho^{(i-1)}_{z_f}(z',r)$ are foreknown, we can derive $\theta^{(i)}_{z_f}(z',r)$ from eq.(19), with eq.(18) substituted in, by setting t to be t_i. Given the thermal conductivity κ=1.5×10^{-3} J/(s×cm×K), equilibrium density ρ_e=1.26 g/cm^3 (pertaining to equilibrium temperature of θ_e=298 K) and c_p=1.0 J/(g×K) for CS_2 [26], the thermal diffusivity coefficient $D_{th}=\kappa/(\rho_e\times c_p)$ for CS_2 is calculated to be 1.2×10^{-3} cm^2/s. This leads to the thermal diffusivity time constant of $\tau_{th}=w_0^2/4D_{th}$=408 μs.

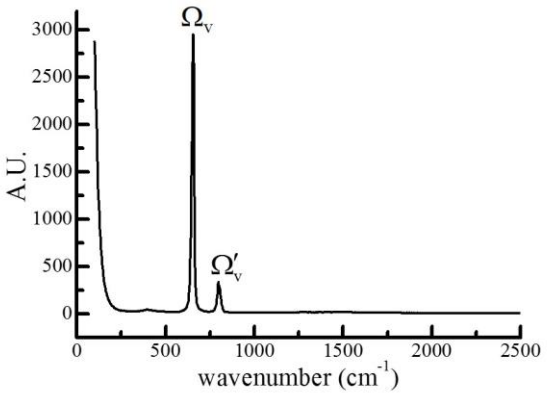

Fig. 5. Vibrations-induced Raman scattering spectrum of liquid CS_2. The strong band centered at 1.2×10^{14} s^{-1} (656 cm^{-1}) (Ω_v) is due to the symmetric stretching mode of the molecule. The weak band centered at 1.5×10^{14} s^{-1} (800 cm^{-1}) (Ω'_v) is due to the overtone of the bending modes. The asymmetric stretching and the bending modes are Raman inactive and do not show Raman scattering signals [33].

Based on $\theta_{z_f}(z',r,t)$ evaluated from eq.(19), we can further derive the sample density $\rho_{z_f}(z',r,t)$ by solving the $\nabla\theta_{z_f}(z',r,t)$-driven thermal acoustic wave equation [28]

$$\frac{\partial^2\rho_{z_f}(z',r,t)}{\partial t^2} - v_s^2\nabla^2\left[\rho_{z_f}(z',r,t)\right] = bv_s^2\rho_{z_f}(z',r,t)\nabla^2\left[\theta_{z_f}(z',r,t)\right] \quad (20)$$

which is valid for t ranging between t_{i-1} and t_i. Here v_s (1149 m/s) and b (1.19×10^{-3} K^{-1}) denote the sound speed and volume expansivity of CS_2 [26]. Since all the 10 data measuring times relative to the leading pulse (T's), ranging between 1 and 41 ms, are much longer than the transit-time $\tau_{ac}=w_0/v_s$=14.0 μm/1149 m/s=12.2 ns, the first term on the left hand side of eq.(20) can be ignored in this study [28]. This leads to

$$\frac{\partial\rho_{z_f}(z',r,t)}{\partial\theta_{z_f}(z',r,t)} = -b\rho_{z_f}(z',r,t) \quad (21)$$

from which we can derive $\rho^{(i)}_{z_f} = \rho^{(i-1)}_{z_f}\times\exp\{-b[\theta^{(i)}_{z_f}-\theta^{(i-1)}_{z_f}]\}$ and hence $\rho^{(i)}_{z_f} = \rho^{(0)}_{z_f}(z',r)\times\exp\{-b[\theta^{(i)}_{z_f}-\theta_e]\}$. Given $\theta^{(0)}_{z_f}(z',r)=\theta_e$ and $\rho^{(0)}_{z_f}(z',r)=\rho_e$ we can solve eqs.(19) and (21) with i advanced from 1 to i_{end}. The initial conditions $\theta^{(i-1)}_{z_f}(z',r)$ and $\rho^{(i-1)}_{z_f}(z',r)$ of eq.(19) for any specific i≥1 are predetermined from earlier calculation of eqs.(19) and (21) pertaining to smaller i's.

When $\Delta\theta^{(i)}_{z_f} \equiv \theta^{(i)}_{z_f} - \theta_e$ and $\Delta\rho^{(i)}_{z_f} \equiv \rho^{(i)}_{z_f} - \rho_e$ contribute to $\Delta n^{(i)}_{z_f}$ cooperatively, $\Delta\rho^{(i)}_{z_f}$ predominates over $\Delta\theta^{(i)}_{z_f}$ [28]. Hence

$$\Delta n^{(i)}_{z_f}(z',r) = \left(\frac{\partial n}{\partial\theta}\right)_{\rho}\Delta\theta^{(i)}_{z_f}(z',r) + \left(\frac{\partial n}{\partial\rho}\right)_{\theta}\Delta\rho^{(i)}_{z_f}(z',r) \cong -\frac{b\gamma^e}{2n}\Delta\theta^{(i)}_{z_f}(z',r) \quad (22)$$

where $(\partial n/\partial\rho)_\theta = \gamma^e/2n\rho_e$ [28] is used with γ^e and n denoting CS_2's electrostrictive coupling constant and linear refractive index. Given $\gamma^e=(n^2-1)(n^2+2)/3$ [28] and n=1.63, $b\gamma^e/2n$ is calculated to be 9.4×10^{-4} K^{-1}. In eq.(22) $\Delta\rho_{z_f}^{(i)}$ is approximated to be $-\rho_e b\Delta\theta_{z_f}^{(i)}$. Mimicking the intensity distribution of a TEM_{00} mode laser pulse, $\Delta\theta_{z_f}^{(i)}$ is nearly Gaussian distributed in r with a maximum at r=0. This ensures that $\Delta n_{z_f}^{(i)}$ is negative with a minimum at r=0, which results in a negative lensing effect for the ith pulse (i>0). $\Delta n_{z_f}^{(i)}$ strengthens with increasing $T_i\equiv t_i-t_0$ within τ_{th} due to cross-pulse heat accumulation and then turns steady with increasing T_i exceeding τ_{th} because heat accumulation is gradually balanced by thermal diffusivity (see eqs.(19) and (22)).

Fig. 5. shows the characteristic energy levels of excited vibrations of CS_2 derived from the measured Raman scattering spectrum. $\Omega_v=1.2\times10^{14}$ s^{-1} (656 cm^{-1} in wavenumber) corresponds to the symmetric stretching mode and $\Omega'_v=1.5\times10^{14}$ s^{-1} (800 cm^{-1} in wavenumber) corresponds to the overtone of the bending mode. Ω_v and Ω'_v are obtained by subtracting the measured angular frequencies of the Raman scattering signals from that of the monochromatic exciting wave.

We anticipate that a transform limited 18 fs-pulse, with $\Delta\omega=5.5\times10^{13}$ s^{-1} considerably smaller than Ω_v, can hardly excite CS_2 molecules from $|0\rangle_v$ to $|1\rangle_v$ via SRS. This agrees with the studies by Nelson, Heisler, Sato and Huang which did not show the OKE signals of CS_2 arising from excitation of vibrations by 60, 100, 100 and 28 fs pulses respectively [16–18,22,23]. Moreover, refs.[18,22,23] further showed the OKE signals due to excitation of the inter-molecular motions: libration, diffusive reorientation and polarizability distortion. Here the OKE signals are proportional to the convolution of the pulses' autocorrelation function and the response functions corresponding to excitation of the molecular motions under consideration. To precisely compare the OKE signal due to excitation of each inter-molecular motion by 18-fs laser pulses used in this study, we simulate, in Part B of the SI, the OKE signals based on the autocorrelation function of our 18 fs-laser pulses ($\exp[-(t/\tau)^2]$) and the response functions shown in ref.[18]. As a result, we find that the signal for libration is considerably stronger than those for diffusive reorientation and polarizability distortion in the time extent within a pulse-duration centered at zero delay (see Fig. S1 in the SI). This ensures that $|\beta_l^2+n_{2l}^2|^{1/2}$ (equivalently $|\beta_h^2+n_{2h}^2|^{1/2}$) for libration dominates over those for diffusive reorientation and polarizability distortion respectively. By further assuming β_l (equivalently β_h) itself for libration dominates over those for the other two inter-molecular motions, we infer, via eqs.(15) and (17), that relaxation of excited libration predominantly contributes to the thermal lensing effect.

Note that although Fig. S1 in the SI shows that the OKE signals reach their maxima at delay times a few times longer than the pulse duration, we pay special attention to the signals at delay time ~0. This is because NLA and NLR due to excitation of these molecular motions are only allowed to evolve for a time about the pulse duration in this study.

4. Computational details

To simulate both the open aperture and closed aperture Z-scan curves measured at each of the 10 times relative to the leading pulse (T's), ranging between 1 and 41 ms, we numerically

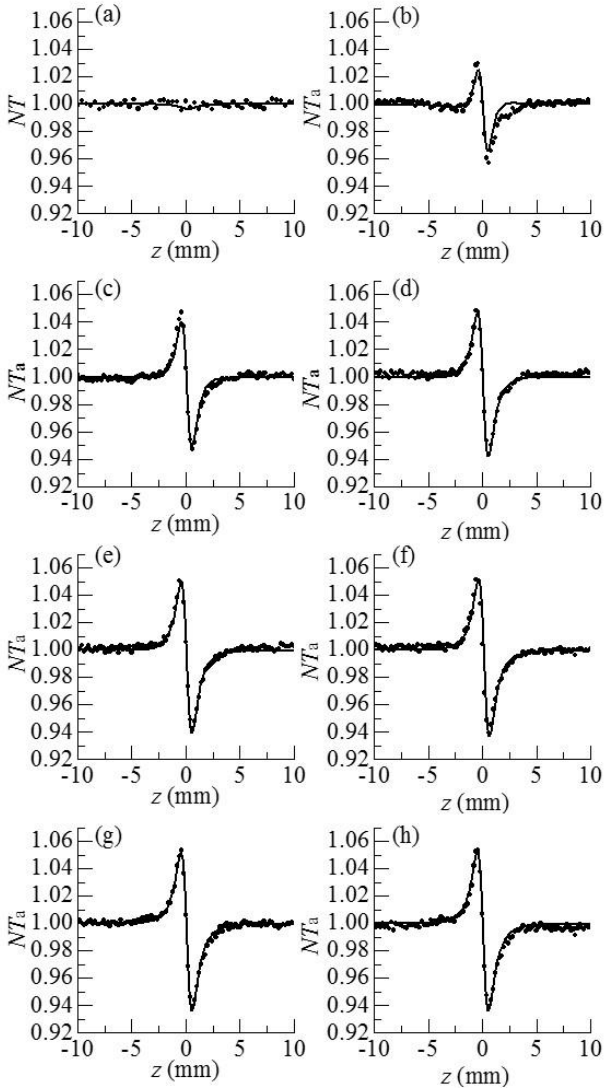

Fig. 6. (a) Open and (b)-(h) closed aperture Z-scan curves of CS_2. The dots and lines in (b)-(h) respectively show the experimental results and theoretical fits executed at 7 times relative to the leading pulse: T=1, 3, 7, 11, 21, 31, and 41 ms. The data taken at T=2, 5, and 9 ms are omitted for conciseness. The Z-scan curves acquired with 240 mW laser pulses are not shown.

integrate eqs.(15) and (16) over z' from 0 to L, given the sample's front surface at any position z_f, for the ith pulse ($0\le i\le i_{end}$). By doing so, we derive the frequency-domain intensity $I'^{(i)}_{z_f}(L,r,\omega)$ and phase $\phi^{(i)}_{z_f}(L,r,\omega)$ (equivalently $\vec{E}''^{(i)}_{z_f}(L,r,\omega)$ and $\vec{E}'^{(i)}_{z_f}(L,r,\omega) = \vec{E}''^{(i)}_{z_f}(L,r,\omega)\times\exp\{-i[k(z_f+L)+\omega T_i]\}$) at the exit surface of the sample. For i>0, we need to conduct the integration or calculation in eqs.(17)-(19), (21) and (22) beforehand. This yields $\Delta n_{z_f}^{(i)}$ involved in eq.(16). However, for the leading pulse (i=0), we simply substitute $\Delta n_{z_f}^{(0)}=0$ into eq.(16) before we integrate eqs.(15) and (16). The incident frequency-domain intensity $I'^{(i)}_{z_f}(0,r,\omega)$ and phase $\phi^{(i)}_{z_f}(0,r,\omega)$ (equivalently the incident electric field $\vec{E}''^{(i)}_{z_f}(0,r,\omega)$ and $\vec{E}'^{(i)}_{z_f}(0,r,\omega) = \vec{E}''^{(i)}_{z_f}(0,r,\omega)\times\exp\{-i[k(z_f+0)+\omega T_i]\}$) are given by eqs.(6) and

(3)). The value of the axial peak intensity $I'_0{}^{(i)}(0,0,\omega_c)$ in eq.(6) is derived from eq.(9) with the incident pulse energy $\varepsilon_0{}^{(i)}=P_{avg}/82$ MHz.

By invoking the Huygens-Fresnel propagation formalism [34], we deduce the frequency-domain intensity at the aperture $I'_a{}^{(i)}$ from $\tilde{E}''^{(i)}_{z_f}(L,r,\omega)$. By integrating $2I''^{(i)}_{z_f}(L,r,\omega)$ over ω from 0 to ∞ and the whole beam cross section, we obtain the total transmitted pulse energy $\varepsilon_t{}^{(i)}$ (see eqs.(7) and (8) for the integration details). By integrating $2I'_a{}^{(i)}$ over ω from 0 to ∞ and the aperture area, we obtain the axial transmitted pulse energy $\varepsilon_a{}^{(i)}$. Given the response function of the detectors (output of an incident delta function $\delta(T)$) $h(T)=0$ for $T\le 0$ and $\exp(-T/20\ \mu s)$ for $T>0$, we further simulate the output powers $P1(T)=h(T)*\sum_{i=0}^{i_{end}}\varepsilon_0^{(i)}\delta(T-T_i)$, $P2(T)=h(T)*\sum_{i=0}^{i_{end}}\varepsilon_t^{(i)}\delta(T-T_i)$ and $P3(T)=h(T)*\sum_{i=0}^{i_{end}}\varepsilon_a^{(i)}\delta(T-T_i)$ to be compared with the experimentally measured D1, D2 and D3. Here "*" denotes the convolution operation, $T_i\equiv(i-1)\times\tau_{p\text{-}p}$ is the arrival time of the i^{th} pulse, relative to the leading pulse, at the sample and T is sequentially set to be each of the data measuring times (T=1, 2, 3, 5, 7, 9, 11, 21, 31 and 41 ms) in P1(T), P2(T) and P3(T) after the convolution operation is completed. Plots of $P2(T)/P1(T)$ and $P3(T)/P1(T)$, after being normalized with those in the linear regime, as functions of z yield the simulated open aperture and closed aperture Z-scan curves.

5. Results and discussion

The normalized open aperture Z-scan curve obtained with un-modulated 18 fs-pulses at P_{avg}=270 mW (equivalently $\varepsilon_0{}^{(i)}=3.3\times10^{-9}$ J) is shown by dots in Fig. 6(a). Exhibiting no discernable structures at around z=0, this curve suggests that CS_2 does not show noticeable NLA or else our Z-scan is not sensitive enough to detect the weak NLA. The dots in Fig. 6(b)-(h) show the normalized closed aperture Z-scan curves measured with 82 MHz 18 fs-pulses (at P_{avg}=270 mW) chopped into trains with a train-width of τ_t=41 ms and a train-to-train separation of $\tau_{t\text{-}t}$=0.18 s. Each of the 7 frames pertains to a measuring time relative to the leading pulse of the train: T=1, 3, 7, 11, 21, 31, and 41 ms, respectively. The measurements conducted at T=2, 5, and 9 ms are omitted in this figure. Appearance of a peak and a valley on the $-z$ and $+z$ sides in each curve indicates a negative lensing effect of the sample (CS_2). When the magnitude of the lensing effect is represented by the difference between the peak and valley values of NT_a in a normalized closed aperture Z-scan curve, which is denoted by $\Delta T_{p\text{-}v}$, we exhibit $\Delta T_{p\text{-}v}$'s, extracted from Fig. 6(b)-(h), by red dots in Fig. 7 as a function of time relative to the leading pulse (T). It is evident that $\Delta T_{p\text{-}v}$'s increase with increasing T within τ_{th}=408 μs and gradually turns steady after T exceeds τ_{th}. This suggests the contribution of thermal lensing effect to the dots in Fig. 6(b)-(h). As depicted by eqs.(17)-(19), (21) and (22), this effect is first accumulated across neighboring pulses and then balanced by thermal diffusivity gradually. Accordingly, when Fig. 6(a) exhibits no discernable structures at around z=0, we assume that NLA of CS_2 is too weak to be observed with our power measuring system. Since the sample thickness 0.1 cm is greatly smaller than the scanned range 2 cm (see the horizontal axes of Fig. 6), we do not rigidly label the sample position by z_f. Instead, we use z, ranging between z_f and z_f+L, to denote the sample position.

The best fits to the dots in Fig. 6(b)-(h), as shown by the solid lines, are obtained with β_l=0.7 cm^2/(W×s) and n_{2l}=0.9 cm^2/ (W×s)

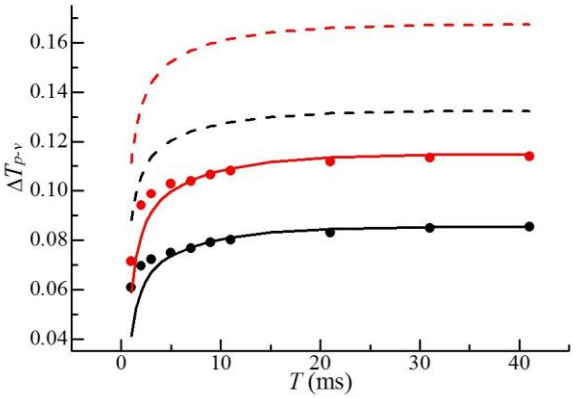

Fig. 7. Plots of $\Delta T_{p\text{-}v}$'s as functions of T: experimental results (dots) and theoretical simulations including the thermal lensing effect and the third-order NLR (the solid lines). The dashed lines correspond to the solid lines with the third-order NLR removed. The red and black symbols pertain to P_{avg} equal to 270 mW and 240 mW respectively.

(i.e., $\tilde{\chi}^{(3)}_{Im}(\omega;\omega,\omega_l,-\omega_l)=-2.8\times10^{-6}$cm^2/(V$^2\times$s) and $\tilde{\chi}^{(3)}_{Re}(\omega;\omega,\omega_l,-\omega_l)=3.7\times10^{-6}$ cm^2/(V$^2\times$s)) for ω_l falling within the range [$\omega-\Omega_l-\Delta\Omega_l/2$, $\omega-\Omega_l+\Delta\Omega_l/2$]. Both β_l and n_{2l} equal 0 (i.e., $\tilde{\chi}^{(3)}_{Im}(\omega;\omega,\omega_l,-\omega_l)$ and $\tilde{\chi}^{(3)}_{Re}(\omega;\omega,\omega_l,-\omega_l)$ equal 0) for ω_l falling outside this range. Synchronously, we use $\beta_h=-\beta_l=-0.7$ cm^2/(W×s) and $n_{2h}=n_{2l}=0.9$ cm^2/(W×s) (i.e., $\tilde{\chi}^{(3)}_{Im}(\omega;\omega,\omega_h,-\omega_h)=2.8\times10^{-6}$ cm^2/(V$^2\times$s) and $\tilde{\chi}^{(3)}_{Re}(\omega;\omega,\omega_h,-\omega_h)=3.7\times10^{-6}$ cm^2/(V$^2\times$s)) for ω_h falling within the range [$\omega+\Omega_l-\Delta\Omega_l/2$, $\omega+\Omega_l+\Delta\Omega_l/2$]. Both β_h and n_{2h} equal 0 (i.e., $\tilde{\chi}^{(3)}_{Im}(\omega;\omega,\omega_h,-\omega_h)$ and $\tilde{\chi}^{(3)}_{Re}(\omega;\omega,\omega_h,-\omega_h)$ equal 0) for ω_h falling outside this range. Here $\Omega_l=3.3\times10^{12}$ s^{-1} (35 cm^{-1} in wavenumber) and $\Delta\Omega_l=3.6\times10^{12}$ s^{-1} (38 cm^{-1} in wavenumber) pertain to libration of CS_2 [35]. Since the spectrum width of $\tilde{E}''^{(i)}_{z_f}(z',r,\omega)$ ($\Delta\omega=5.5\times10^{13}$ s^{-1}) is considerably larger than Ω_l, we can find ω in a wide extent of the spectrum of $\tilde{E}''^{(i)}_{z_f}(z',r,\omega)$ with ω_l within the range [$\omega-\Omega_l-\Delta\Omega_l/2$, $\omega-\Omega_l+\Delta\Omega_l/2$] or ω_h within the range [$\omega+\Omega_l-\Delta\Omega_l/2$, $\omega+\Omega_l+\Delta\Omega_l/2$] covered in the spectrum of $\tilde{E}''^{(i)}_{z_f}(z',r,\omega)$ with ω. Note that when the simulated open aperture Z-scan curve (the solid line in Fig. 6(a)) shows a weak dip at $z\sim0$ with the depth within the fluctuation of the dots, it is closely comparable with the dots at each z. This indicates that weak NLA of each individual pulse by CS_2 builds up an observable thermal lensing effect in virtue of heat accumulation across millions of pulses (41 ms/12.2 ns~3.4 million). The red line in Fig. 7 is extracted from the solid lines in Fig. 6(b)-(h). The black dots and solid line shown in Fig. 7 are the experimental and theoretical results, corresponding to P_{avg}=240 mW (equivalently $\varepsilon_0{}^{(i)}=2.9\times10^{-9}$ J), obtained in the same manner as the red dots and solid line. However, the Z-scan results obtained at this average power are not shown in this work.

By removing the third order NLR from the solid lines in Fig. 7, we obtain the dashed lines to reflect the thermal lensing effect alone. As a result, we find the ratio of the red one (corresponding to P_{avg}=270 mW) to the black one (corresponding to P_{avg}=240

mW) equals the ratio of the corresponding P_{avg}'s (270 mW/240 mW) to the second power. This ensures that heat is generated by third order NLA [5,6].

Given the Avogadro constant N_a=6.02×10^{23} mole^{-1} as well as equilibrium density ρ_e=1.26 g/cm^3 and molecular weight M=76.14 g/mole for CS_2, we obtain the equilibrium molecular concentration 1.0×10^{22} cm^{-3} for CS_2 residing on $|0\rangle_l$. On the other hand, division of $\delta Q^{(i)}_{z_i=0}(z'=0,r=0)$, pertaining to P_{avg}= 270 mW, by $\hbar\Omega_l$ yields the maximal possible molecular concentration 9.3×10^{18} cm^{-3} for CS_2 promoted to $|1\rangle_l$ state. Since it is greatly smaller than the equilibrium one on $|0\rangle_l$, we ignore anti-Stoke SRS in this study.

Note that two things about our simulation can be improved in the future. First of all, by assuming n_{2l}=n_{2h}=0.9 cm^2/ (W×s) in our simulation, we have fitted the observed negative lensing effect based on the thermal lensing effect and third order NLR in this study. In the future, we will repeat the same measurements conducted in this study once 18 fs-laser pulses with a pulse-to-pulse separation $\tau_{p\text{-}p}$ considerably longer than the thermal diffusivity time constant τ_{th} become available. With the cross-pulse accumulated thermal lensing effect eliminated, the results are expected to yield the sign and magnitude of n_{2l} and n_{2h} with more accuracy. By the way, if a regenerative amplifier is used to generate the desired 18 fs-laser pulses, we can additionally evaluate β_l and β_h more accurately by properly turning up the pulse energy. With more reliable n_{2l}, n_{2h}, β_l and β_h determined, we can improve the evaluation of thermal lensing effect made in this study. Secondly, we have assumed that n_{2l}, n_{2h}, β_l and β_h are constants for ω_l and ω_h falling within the ranges [ω–Ω_l–$\Delta\Omega_l$/2, ω–Ω_l+$\Delta\Omega_l$/2] and [ω+Ω_l–$\Delta\Omega_l$/2, ω+Ω_l+$\Delta\Omega_l$/2] respectively and equal 0 otherwise. In the future, we will derive $\tilde{\chi}^{(3)}(\omega;\omega,\omega_l,-\omega_l)$ and $\tilde{\chi}^{(3)}(\omega;\omega,\omega_h,-\omega_h)$ as functions of (ω–ω_l–Ω_l) and (ω–ω_h+Ω_l), e.g., Lorentzian functions of (ω–ω_l–Ω_l) and (ω–ω_h+Ω_l) [29]. The results will depict the dispersions of $\tilde{\chi}^{(3)}(\omega;\omega,\omega_l,-\omega_l)$ and $\tilde{\chi}^{(3)}(\omega;\omega,\omega_h,-\omega_h)$ (equivalently β_l and n_{2l} as well as β_h and n_{2h}).

The thermal lensing effect observed in simple liquids may additionally involve the contribution of contaminant absorption [36]. However, this suspected contaminated absorption has been excluded in this study by using spectral grade CS_2 sample and further examining it with analytical methods including high-performance liquid chromatography and gas chromatography-mass spectrometry.

6. Conclusion

In summary, we have experimentally verified the thermal lensing effect induced in CS_2 by 820 nm 18 fs-laser pulses at a repetition rate of 82 MHz. In addition, we have quantitatively interpreted this effect in the light of relaxation of excited libration. This mechanism differs from the common view of relaxation subsequent to multi-photon excitation processes.

Acknowledgements

T. H. Wei gratefully acknowledges financial support from National Science Council grant NSC 102-2112-M-194-002-MY3 and from Ministry of Economic Affairs grant 94-EC-17-A-08-S1-0006, Taiwan. T. H. Wei also thanks E. W. Van Stryland of CREOL, University of Central Florida, for helpful discussions. C. I. Lee is grateful to Ministry of Science and Technology for financial support (MOST 103-2113-M-194-008).

Notes and references

[a] Department of Physics, National Chung Cheng University, Min-Hsiung, Chia-Yi 621, Taiwan, Republic of China.
[b] #1323, 5115 Garden City Rd., Richmond, BC V6X4H6, Canada.
[c] Department of Life Science, National Chung Cheng University, Min-Hsiung, Chia-Yi 621, Taiwan, Republic of China.
† Corresponding author: 886-95-309-1670; (05) 272-0411 ext. 66324; E-mail address: twei@ccu.edu.tw. (05) 272-0411 ext. 66511; E-mail address: biocil@ccu.edu.tw.

1 M. Falconieri, and G. Salvetti, *Simultaneous measurement of pure-optical and thermo-optical monlinearities induced by high-repetition-rate, femtosecond laser pulses: application to CS_2*, Appl. Phys. **B**, 1999, **69**, 133.
2 S. Couris, M. Renard, O. Faucher, B. Lavorel, R. Chaux, E. Koudoumas, and X. Michaut, *An experimental investigation of the nonlinear refractive index (n_2) of carbon disulfide and toluene by spectral shearing interferometry and z-scan techniques*, Chem. Phys. Lett. 2003, **369**, 318.
3 K. Kamada, K. Matsunaga, A. Yoshino, and K. Ohta, *Two-photon-absorption accumulated thermal effect on femtosecond Z-scan experiments studied with time-resolved thermal-lens spectrometry and its simulation*, J. Opt. Soc. Am. **B**, 2003, **20**, 529.
4 R. A. Ganeev, A. I. Ryasknynsky, M. Baba, M. Suzuki, N. Ishizawa, M. Turu, S. Sakakibara and H. Kuroda, *Nonlinear refraction in CS_2*, Appl. Phys. **B**, 2004, **78**, 433.
5 A. Gnoli, L. Razzari and M. Righini, *Z-scan measurements using high repetition rate lasers: how to manage thermal effects*, Opt. Express, 2005, **13**, 7976-7981.
6 M. Falconieri, *Thermo-optical effects in Z-scan measurement using high-repetition-rate lasers*, J. Opt. A: Pure Appl. Opt., 1999, **1**, 662.
7 Yi-Ci Li, Sou-Zi Kuo, Tai-Huei Wei, Jian-Neng Wang, Sidney S. Yang, and Jaw-Luen Tang, *Control of thermal lensing effect in transparent liquids by femtosecond laser pulses*, Jpn. J. Appl. Phys., 2009, **48**, 09LF06.
8 M. Sheik-Bahae, A. A. Said, T. H. Wei, D. J. Hagan, and E. W. Van Stryland, *Sensitive measurement of optical nonlinearities using a single beam*, IEEE J. Quantum Electron., 1990, **26**, 760.
9 R. W. Boyd, *Nonlinear Optics*, (Academic Press, New York, 1992), p. 372.
10 Y. X. Yan, and K.A. Nelson, *Impulsive stimulated light scattering. I. General theory*, J. Chem. Phys., 1987, **87**, 6240.
11 W. Lotshaw, D. McMorrow, C. Kalpouzos, and G. A. Kenney-Wallace, *Femtosecond dynamics of the optical kerr effect in liquid nitrobenzene and chlorobenzene*, Chem. Phys. Lett., 1987, **136**, 323.
12 S. J. Rosenthal, N. F. Scherer, M. Cho, X. Xie, M. E. Schmidt, and G. R. Fleming, in *Ultrafast Phenomena*, edited by J. L. Martin, A. Migus, G. A. Mourou, and A. H. Zewail (Springer, Berlin, 1993), Vol. 8, p. 616.
13 T. H. Huang, C. C. Hsu, T. H. Wei, M. J. Chen, S. Chang, W. S. Tse, H. P. Chiang, and C. T. Kuo, *The ultrafast dynamics of liquid $CBrCl_3$ studied with optical Kerr effect and Raman scattering*, Mol. Phys., 1999, **96**, 389.

14 J. L. Tang, C. W. Chen, J. Y. Lin, Y. D. Lin, C. C. Hsu, T. H. Wei, and T. H. Huang, *Ultrafast motion of liquids $C_2H_4Cl_2$ and $C_2H_4Br_2$ studied with a femtosecond laser*, Optics Commun., 2006, **266**, 669.
15 N. A. Smith and S. R. Meech, *Optically-heterodyne-detected optical Kerr effect (OHD-OKE): applications in condensed phase dynamics*, Int. Rev. Phys. Chem., 2002, **21**, 75.
16 S. Ruhman, A. G. Joly, B. Kohler, L. R. Williams, and K. A. Nelson, *Intramolecular and intermolecular dynamics in molecular liquids through femtosecond time-resolved impulsive stimulated scattering*, Revue Phys. Appl., 1987, **22**, 1717.
17 S. Ruhman, B. Kohler, A. G. Joly, and K. A. Nelson, *Molecular dynamics in liquids from femtosecond time-resolved impulsive stimulated scattering*, IEEE J. Quantum. Electron., 1988, **24**, 470.
18 I. A. Haisler, R. R. B. Correia, T. Buckup, S. L. S. Cunha, and N. P. da Silveira, *Time-resolved optical Kerr-effect investigation on CS_2/polystyrene mixtures*, J. Chem. Phys., 2005, **123**, 054509.
19 D. McMorrow, N. Thantu, J. S. Melinger, S. K. Kim, and W. T. Lotshaw, *Probing the microscopic molecular environment in liquids: Intermolecular dynamics of CS_2 in alkane solvents*, J. Phys. Chem., 1996, **100**, 10389.
20 B. Kohler, and K. A. Nelson, *Femtosecond molecular dynamics of liquid carbon disulphide at high pressure*, J. Phys.: Condens. Matter, 1990, **2**, SA109.
21 A. Tokmakoff, and G. R. Fleming, *Two-dimensional Raman spectroscopy of the intermolecular modes of liquid CS_2*, J. Chem. Phys., 1997, **106**, 2569.
22 Y. Sato, R. Morita, and M. Yamashita, *Study on ultrafast dynamics behaviors of different nonlinear refractive index components in CS_2 using a femtosecond interferometer*, Jpn. J. Appl. Phys., 1997, **36**, 2109.
23 T. H. Huang, C. C. Hsu, T. H. Wei, S. Chang, S. M. Yen, C. P. Tsai, R. T. Liu, C. T. Kuo, W. S. Tse, and C. Chia, *The transient optical Kerr effect of simple liquids studied with an ultrashort laser with variable pulsewidth*, IEEE J. Sel. Topics Quantum Electron., 1996, **2**, 756.
24 Y. R. Shen, *The Principles of Nonlinear Optics*, (Wiley-Interscience, New York, 1984), Chaps. 10 and 11.
25 M. Denariez, and G. Bret, *Investigation of Rayleigh wing and Brillouin-stimulated scattering in liquids*, Phys. Rev., 1968, **171**, 160.
26 D. R. Lide (ed.), *CRC handbook of Chemistry and Physics*, 83rd ed., (CRC Press, Boca Raton, 1996).
27 D. I. Kovsh, S. Yang, D. J. Hagan, and E. W. Van Stryland, *Nonlinear optical beam propagation for optical limiting*, Appl. Opt., 1999, **38**, 5168.
28 D. I. Kovsh, D. J. Hagan and E. W. Van Stryland, *Numerical modeling of thermal refraction inliquids in the transient regime*, Opt. Express, 1999, **4**, 315.
29 M. Schubert, and B. Wilhelmi, *Nonlinear Optics and Quantum electronics*, (Wiley, 1986), p. 107.
30 A. Yariv, *Optical Electronics*, (Oxford University Press, New York, 1990), Chap. 2.
31 J.-C. M. Diels, J. J. Fontaine, I. C. McMichael, and F. Simoni, *Control and measurement of ultrashort pulse shapes (in amplitude and phase) with femtosecond accuracy*, Appl. Opt., 1985, **24**, 1270.
32 P. N. Butcher, and D. Cotter, *The Element of Nonlinear Optics*, (Cambridge, 1990), Chap. 7.
33 D. Wang, K. Mittauer, and N. Reynolds, *Raman scattering of carbon disulphide: The temperature effect*, Am. J. Phys., 2009, **77**, 1130.
34 M. Born, and E. Wolf, *Principles of Optics*, 5th ed., (Pergamon, 1975), p. 383.
35 D. McMorrow, W. T. Lotshaw, and G. A. Kenney-Wallace, *Temporal evolution of the vibrational normal modes in halogenated methanes*, Chem. Phys. Lett., 1988, **145**, 309.
36 M. Samoc, A. Samoc, B. Luther-Davies, M. G. Humphrey, and M.-S. Wong, *Third-order optical nonlinearities of oligomers, dendrimers and polymers derived from solution Z-scan studies*, Opt. Mater., 2002, **21**, 485.